Crystallographic Stability of Metastable Phase formed by Containerless Processing in REFeO$_3$ (RE: Rare-earth Element)

Kazuhiko Kuribayashi[1, 2], M. S. Vijaya Kumar[2]

[1] Shibaura Institute of Technology,
Toyosu, Koto, Tokyo 135-8548, Japan
[2] Institute of Space and Astronautical Science, JAXA,
Yoshinodai, Sagamihara, Kanagawa 252-5210, Japan

Abstract

Undercooling a melt often facilitates a metastable phase to nucleate preferentially. Although the classical nucleation theory shows that the most critical factor for forming a metastable phase is the interface free energy, the crystallographic stability is also indispensable for the phase to be frozen at ambient temperature. In compound materials such as oxides, authors have suggested that the decisive factors for forming a critical nucleus are not only the free energy difference but also the difference of the entropy of fusion between stable and metastable phases. In the present study, using REFeO$_3$ (RE: rare-earth element) as a model material, we investigate the formation of a metastable phase from undercooled melts with respect to the competitive nucleation and crystallographical stabilities of both phases.

Introduction

A metastable phase is a phase that does not exist in thermal equilibrium state and, although thermodynamically unstable, can temporarily exist when some conditions are fulfilled. Research into the metastable phase began with Ostwald's prediction that a phase formed first from supersaturated liquid is not always thermodynamically stable but is close to liquid in energy [1]. This prediction is called "step rule". Later on, Stranski and Totomanov [2] suggested that the step rule is a consequence of preferential formation of a critical nucleus of the metastable phase. That is, the activation energy required to form a critical nucleus, ΔG_n^*, controls the nature of the process. Regarding this point, the classical nucleation theory [3] states that ΔG_n^* can be understood in terms of the interfacial free energy γ between the liquid and solid phases. Turnbull [4] and Spaepen [5], assuming that γ of a simple material such as metal is related not to the enthalpy change but to the entropy change at the solid–liquid interface, formulated γ as

$$\gamma = \alpha \frac{\Delta S_f T}{\left(N_A V_m^2\right)^{\frac{1}{3}}},$$ (1)

where ΔS_f, T, N_A and V_m are the heat of fusion, the temperature of material, Avogadro number and the molar volume, respectively. Furthermore, Spaepen and Meyer [6] derived α, dimensionless solid-liquid interfacial energy, as 0.86 for fcc or hcp crystals and 0.71 for bcc structures, respectively. The α–factors, which strongly depend on the structure of both solid and liquid phase, are to be a critical parameter to determine ΔG_n^*. In fact, it has been reported that the phase selection of the stable γ-phase or the metastable δ-phase in Fe–Ni–Cr alloys is controlled by α [7-9]. However, almost the metastable phases formed at the first recalescence, which

change into the stable phases at the second recalescence, are not frozen into ambient temperature. In order that the metastable phase may be frozen into ambient environment, the nucleation criterion of metastable phase as well as the crystallographical stability must be fulfilled. Then, in the present investigation, using $REFeO_3$ as the model material, where RE means rare-earth elements, the phase selections not only in the nucleation stage but also the growth stage are discussed.

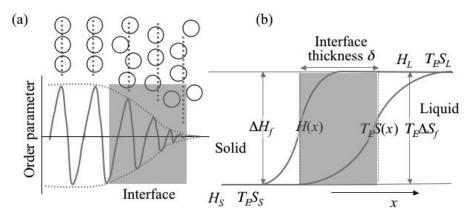*Entropy-undercooling regime criterion of phase selection*

Before taking up the main subject of this paper, we mention again the hypothesis that, in ionic crystals, ΔS_f is to be a dominant factor in the determination of γ.

Spaepen [10] and Granasy [11], almost at the same time, developed rather similar models that γ at equilibrium state is given by
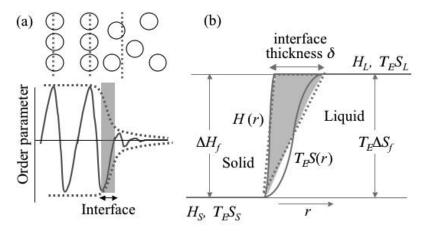
$$\gamma = \int_v \left(H(r) - TS(r) \right) dr ,$$ (2)

where $H(r)$ and $S(r)$ are cross-interfacial enthalpy and entropy. Figure 1 shows a schematical illustration of Eq. 2, where (a) shows the change of the atomic order and of the order parameter in solid and liquid, and (b) schematic representation of the change in the enthalpy $H(r)$ and the product $T_E S(r)$ of melting temperature and entropy at the solid-liquid interface. The colored area corresponds to the approximate value of the interfacial energy, showing that α is not a dimensionless interfacial energy but a dimensionless interface thickness. This model can qualitatively infer the temperature dependence of the solid-liquid interfacial free energy. However, we need analytical or numerical forms of $H(r)$ and $S(r)$ in order to evaluate the interface thickness that is the key parameter of the model.
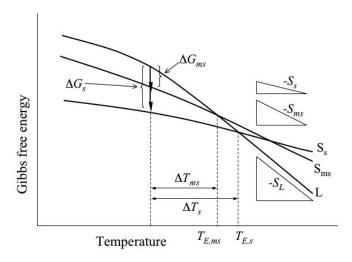
On the other hand, in a material having faceted interface, the order parameter representing the regularity of the atomic arrangement rapidly changes as the interface is crossed as shown in Fig. 2. In this case, $H(r)$ can be approxiomated by the near-step function as shown in Fig. 2(b). Consequently, the interfacial energy is approximated with a triangle if we assume $S(r)$ as a linear function of r at the cross-interface region. This result also means that α is a dimensionless interface thickness rather than a dimensionless interfacial energy. The recent numerical calculation of α based on the molecular dynamics and the density functional analysis suggests

Figure 1. Schematic representation of the nonfaceted interface between solid and liquid. (a) change of the atomic order and of the order parameter in solid and liquid. (b) schematic representation of the change in the enthalpy $H(r)$ and the product $T_E S(r)$ of melting temperature and entropy at the solid-liquid interface. The colored area corresponds to the approximate value of the interfacial energy, showing that α is not a dimensionless interfacial energy but a dimensionless interface thickness.

Figure 2. Schematic representation of the faceted interface between solid and liquid. (a) change of the atomic order and of the order parameter in solid and liquid. (b) schematic representation of the change in $H(r)$ and $T_E S(r)$. The colored area corresponds to the approximate value of the interfacial energy, suggesting the interface thickness is approximately half of the atomic layer spacing.

Figure 3. Schematical image of temperature dependency of free energy in liquid and solid phases (stable and metastable phases). The entropies of three phase are related $S_L > S_{ms} > S_s$. Therefore, as for entropy of fusion ΔS_f caused by solidification, the relation $\Delta S_{f,s} > \Delta S_{f,ms}$ becomes valid.

the interface thickness is approximately half of the atomic layer spacing [12], which implies that the model shown in Fig. 2 is qualitatively valid even in the nonfaceted interface.

Figure 3 schematically shows the thermodynamic relation when considering the step rule [13]. The figure depicts temperature and free energy of both liquid and solid phases (stable and metastable phases). The reason why liquid phase changes to solid phase is that the free energy of the liquid phase becomes larger than that of solid phase. The energy-balance point of both phases is the melting point. Comparing the metastable phase to the stable solid phase in terms of free energy, the free energy of the metastable phase, G_{ms}, is larger than that of stable phase, G_s, (the subscripts s and ms mean stable phase and metastable phase, respectively). Therefore, the melting point of the metastable phase, $T_{E,ms}$, becomes lower than that of stable phase, $T_{E,s}$. Meanwhile,

the absolute value of the gradient of each curve (temperature coefficient of Gibbs free energy) in Fig. 2 corresponds to the entropy when pressure is constant. From the figure, we can see the relation $S_L > S_{ms} > S_s$ between entropies of liquid phase S_L, stable phase S_s and metastable phase S_{ms}. Therefore, for the change of entropy, ΔS_f, caused by melting, we can find a relation $\Delta S_{f,s} > \Delta S_{f,ms}$ (i.e., the change of the entropy is smaller when the liquid phase changes to metastable phase). From the relative relations of the three phases above, we can see that the metastable phase is to be a higher entropy phase than the stable phase [14].

Factors determining the entropy of material are first, density of material and secondly, symmetry of arrangement of atoms and/or molecules making up the material. Therefore, high entropy phase is liquid rather than solid, and gas rather than liquid. Among solid phases, it is guessed that the low-density phase becomes higher-entropy phase. In conclusion, we can say that the metastable phase is lower density, higher symmetric material than the stable state.
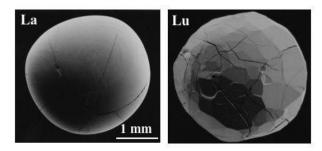
Experimental procedure and results

Spherical samples of REFeO$_3$ were prepared from high purity (99.99%) RE$_2$O$_3$ and Fe$_2$O$_3$ powders. Levitation and melting of samples were carried out by an aerodynamic levitator, ADL, which was designed in order to solidify undercooled melts under the precisely controlled P_{O_2}. Details of the sample preparation and experimental facility are shown elsewhere [15, 16].

Goldschmidt [17] discussed the stability of the perovskite (ABO$_3$) structure using the tolerance factor, TF:

$$TF = \frac{R_A + R_O}{\sqrt{2}\left(R_B + R_O\right)}. \tag{3}$$

In the present investigation, ionic radii of R_A, R_B and R_O correspond to those of rare-earth element, iron and oxygen, respectively. From the systematic investigation, he summarized that the perovskite structure is stable at $TF > 0.8$ and contrary unstable at $TF < 0.8$. Using Shannon ionic radii from La (0.1216 nm) to Lu (0.1032 nm), TF's for the REFeO$_3$ system were calculated to be 0.905 for LaFeO$_3$ to 0.841 for LuFeO$_3$. Therefore, the perovskite structure is expected to be stable in the REFeO$_3$ system.
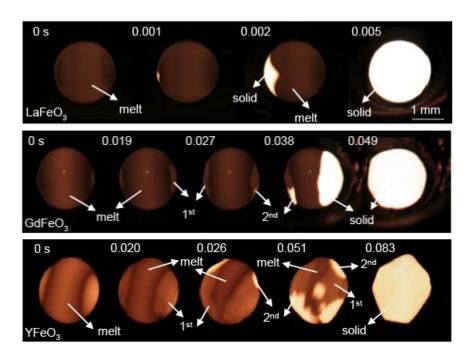
Figure 4 shows SEM micrographs of samples of REFeO$_3$ solidified in containerless conditions. As shown in the photographs, their surface profiles vary according to the type of rare-earth elements. The surface of LaFeO$_3$ is nonfacetted and spherical while that of LuFeO$_3$ is facetted and polyhedral [18]. Note that the different surface features result from differences in crystal structure, not differences in rare-earth element. Specifically, the lattice structure of the LaFeO$_3$ sample is orthorhombic, the space group of which is *Pbnm* (*o*-REFeO$_3$), while the LuFeO$_3$ sample is a hexagonal-symmetric of *P*6$_3$*cm* (*h*-REFeO$_3$). As the *h*-REFeO$_3$ phase has a 10%~20% smaller

Figure 4. Surface profiles of REFeO$_3$ (RE=La, Lu) formed by containerless process. LaFeO$_3$ with large ionic radius has a smooth and spherical surface while LuFeO$_3$ with small radius has a rugged and polyhedral surface.

density than that of perovskite [19], it is estimated that the hexagonal crystal is a higher entropy phase than perovskite. In other words, the hexagonal crystal should have intrinsically become stable perovskite. However, having been largely undercooled to below $T_{E,ms}$ indicated in Fig. 2 by the containerless process, hexagonal crystals of high-entropy phase grew as metastable phase (Fig. 5). In fact, when we forced it to solidify at a temperature of around $T_{E,s}$ even by the same containerless process, stable-phase perovskite appears.

Figure 5 shows typical images taken sequentially during recalescence in samples of $LaFeO_3$, $GdFeO_3$ and $YFeO_3$, each of which is processed at oxygen environment. The elapsed time indicated in each image was set to 0 s for one frame before the nucleation. At oxygen environment, although single recalescence that can be ascribed to the phase transition from undercooled melt to equilibrium perovskite phase was observed in $LaFeO_3$ samples, double recalescences were observed in $GdFeO_3$ and $YFeO_3$ samples, where a primary phase was solidified from the undercooled melt and then the secondary phase with higher brightness was initiated at the interface between melt and the primary phase. The high brightness implies that the melting temperature of the secondary phase was much higher than that of the primary phase. This result indicates that decrease of TF facilitates the undercooled melt to solidify into the metastable h-$REFeO_3$ phase rather than the stable o-$REFeO_3$ phase. According to this result, reduction of the oxygen partial pressure Po_2 is expected to extend the range of TF for metastable h-$REFeO_3$ phase to be formed, because decreasing Po_2 increases the amount of Fe^{2+} (0.078 nm for CN=6) with larger ionic radius than that of Fe^{3+} (0.0645 nm for CN=6).
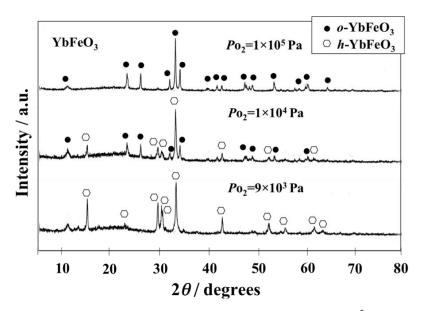

Figure 5. Sequence photographs of HSV images taken during recalescences in the $REFeO_3$ (R = La, Gd and Y) samples processed at oxygen environment. Although in $LaFeO_3$ single recalescence was observed, in $GdFeO_3$ and $YFeO_3$ double recalescences indicating the formation of metastable phases were observed.

In addition, $YbFeO_3$ was used to study the effect of ionic radii of RE elements on the formation of metastable phases, because the ionic radius of Yb^{3+} (0.1042 nm) was slightly larger than that of Lu^{3+} (0.1032 nm). Figure 6 shows the XRD patterns of $YbFeO_3$ samples processed at controlled Po_2. At 10^5 Pa of Po_2, the stable orthorhombic phase (o-$YbFeO_3$) was formed at the second recalescence as in the cases of $GdFeO_3$ and $YFeO_3$. At 10^4 Pa of Po_2, however, the
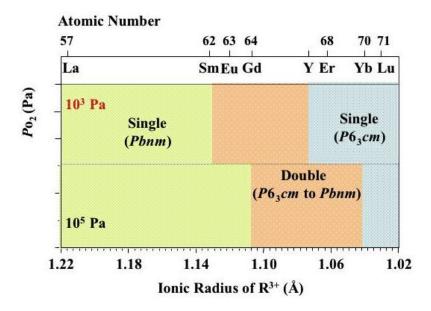
metastable hexagonal phase (h-REFeO$_3$) remained, forming the dual phase with o-YbFeO$_3$, and at 9×10^3 Pa, the o-YbFeO$_3$ phase did not appear [20].

These results suggest that the decrease of Po$_2$ facilitates the undercooled melt to solidify to metastable h-REFeO$_3$ phase rather than the stable o-REFeO$_3$ phase, particularly in samples with RE^{3+} of relatively small ionic radius.

Figure 7 shows the relation between the recalescence results and Po$_2$ as a function of the ionic radii of RE^{3+}, in which Shannon ionic radii for CN=9 were used. Decrease of Po$_2$ extends the

Figure 6. XRD patterns of the YbFeO$_3$ samples processed at Po$_2$=10^5 Pa, Po$_2$=10^4 Pa and Po$_2$=9×10^3 Pa, respectively. At 10^5 Pa of Po$_2$, the stable orthorhombic phase (o-YbFeO$_3$) was formed at the second recalescence as in the cases of GdFeO$_3$ and YFeO$_3$. At 10^4 Pa of Po$_2$, however, the metastable hexagonal phase (h-REFeO$_3$) remaind, forming the dual phase with o-YbFeO$_3$, and at 9×10^3 Pa, the o-YbFeO$_3$ phase did not appear.

Figure 7. Relation between the recalescence results and Po$_2$ as a function of the ionic radii of RE^{3+}, in which Shannon ionic radii for CN=9 were used.

133

range of *TF* for metastable *h*-REFeO$_3$ phase to be formed.

Discussion

Bertaut *et al*. [21] and Yakel *et al*. [22] have first reported the two hexagonal modifications in the ABO$_3$ systems, the space groups of which are *P6$_3$/mmc* and *P6$_3$cm*, respectively. In the *h*-REMnO$_3$ system, the *P6$_3$cm* type modification was formed as a low temperature phase for RE^{3+} with small ionic radius (Ho-Lu, Y and Sc), whereas the *P6$_3$/mmc* type modification was reported as a high temperature phase. In our experiment, although the space group of the metastable *h*-REFeO$_3$ phase belonged to *P6$_3$cm*, the high temperature phase can be deduced to belong to the *P6$_3$/mmc* space group because the ionic radius of Fe^{3+} is as same as that of Mn^{3+} (0.0645 nm for 6 coordination) [23]. Hence, in this investigation, the geometrical analysis of the atomic configuration in *h*-REFeO$_3$ is developed on the assumption that the space group of the primary phase is *P6$_3$/mmc*.

The atomic configuration of the *P6$_3$cm* modification in ABO$_3$ system can be described as a dense oxygen-ion packing (ABCACB) with B^{3+} ions having coordination number CN=5 (five-fold distorted trigonal bipyramidal coordination), and A^{3+} with CN=7 (seven-fold monocapped octahedral coordination), forming a noncentrosymmetric structure. On the other hand, centrosymmetric *P6$_3$/mmc* is assumed to be described simply with B^{3+} ions of undistorted CN=5 and A^{3+} of CN=6 (octahedral coordination).
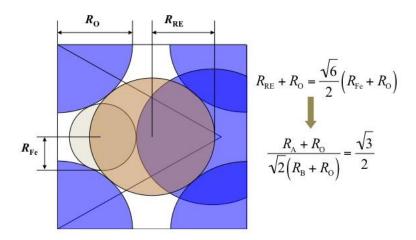
Figure 8 shows the geometrical configuration among RE^{3+}(CN=6), Fe^{3+}(CN=5), and O^{2-} in a space group of *P6$_3$/mmc*, in which the constituent ions are packed without any spacing between neighboring ions. As shown in this figure, the relation among the ionic radii of constituent ions of *h*-REFeO$_3$ is expressed as

$$R_{RE} + R_{O} = \frac{\sqrt{6}}{2}\left(R_{Fe} + R_{O}\right). \tag{4}$$

Therefore, the *h*-REFeO$_3$ phase will be ideal when the next equation is fulfilled,

$$TF = \frac{\sqrt{3}}{2} \approx 0.87 \tag{5}$$

The experimental results showed that the *h*-GdFeO$_3$ phase is formed because *TF* of which is 0.867. Whereas, the *h*-EuFeO$_3$ is not formed because of slightly high *TF* of 0.871. This suggests

$$R_{RE} + R_{O} = \frac{\sqrt{6}}{2}\left(R_{Fe} + R_{O}\right)$$

$$\frac{R_{A} + R_{O}}{\sqrt{2}\left(R_{B} + R_{O}\right)} = \frac{\sqrt{3}}{2}$$

Figure 8. Geometrical configuration among RE^{3+} (CN=6), Fe^{3+} (CN=5), and O^{2-} in a space group of *P6$_3$/mmc*, in which the constituent ions are packed with no space between neighboring ions. The *h*-REFeO$_3$ phase will be the ideal at *TF* = 0.87.

that the aforementioned condition expressed by Eq. 5 is to be the criterion for the metastable *h*-REFeO$_3$ phase to be formed.

Conclusion

Using REFeO$_3$ (RE: rare-earth element) as a model material, containerless solidification for forming a metastable phase from undercooled melts was carried out as a function of Po_2 (oxygen partial pressure). Based on the geometrical consideration on the ionic radii of constituent ion, RE^{3+}, Fe^{3+} and O^{2-}, tit was derived that the criterion for metastable hexagonal phase is also expressed by tolerance factor, *TF*:

$$TF < 0.87.$$

Experimental result well agreed with this criterion under reduced Po_2 as well as for ambient conditions.

References
[1]   W. Ostwald, *Z. Phys. Chem*. **22** (1897) 282.
[2]   I. Stranski and D. Totomanov, *Z. Phys. Chem*. **A 163** (1933) 399.
[3]   K. F. Kelton, *Solid State Physics* **45** (1991) 75.
[4]   D. Turnbull and R. E. Cech, *J. Appl. Phys*. **21** (1950) 804.
[5]   F. Spaepen, *Acta Metall*. **23** (1975) 729.
[6]   F. Spaepen and P. B. Meyer, *Scripta Metall*. **10** (1976) 257.
[7]   Y. −Y. Chuang, C. −C. Hsieh and Y. A. Chen, *Metall. Trans. A*, **17A** (1986) 1361.
[8]   T. Koseki and M. C. Flemings, *Metall. Mater. Trans. A*, **26A** (1995) 2991.
[9]   T. Volkman, W. Loeser and D. M. Herlach, *Metall. Mater. Trans. A*, **28A** (1997) 453.
[10] F. Spaepen, *Solid State Physics*, **47** (1994), p.1.
[11] L. Granasy, *J. Non-Cryst. Solids*, **162** (1993) 301.
[12] D. W. Marr and A. P. Gust, *J. Chem. Phys.* **99** (1993) 2024.
[13] K. Kuribayashi and S. Ozawa, *J. Alloy Compd.* **408-412** (2006) 266.
[14] K. Kuribayashi, K. Nagashio, K. Niwata, M. S. Vijaya Kumar and T. Hibiya, *Mater. Sci. Eng*. **A 449-451** (2007) 675.
[15] K. Nagashio, Y. Takamura, K. Kuribayashi and Y. Shiohara, *J. Crystal Growth* **200** (1999) 118.
[16] M. S Vijaya Kumar, K. Nagashio, T. Hibiya and K. Kuribayashi, *J. Am. Ceram. Soc.* (2008) **91** 806.
[17] V. M. Goldschmidt, *Die Gesetze der Krystallochemie* Math -Naturv. Kl. Oslo, Norway, **8 (1926)** 1.
[18] K. Nagashio and K. Kuribayashi, *J. Am. Ceram. Soc.* **85** (2002) 2550.
[19] A. A. Bosak, C. Dubourdieu, J. -P. Senateur, O. Yu. Gorbenko and A. R. Kaul, *Crystal Engineering* **5** (2002) 355.
[20] M. S. Vijaya Kumar, K. Kuribayashi and K. Kitazono, *J. Am. Ceram. Soc.* **92** (2009) 903.
[21] E. F. Bertaut and J. Mareschal, *Compt. Rend*. **257** (1963) 867.
[22] H. L. Yakel, W. C. Koehler, E. F. Bertaut and E. F. Forrat, *Acta. Cryst*. **16 (1963)** 957.
[23] K. Nagashio, K. Kuribayashi, M. S. Vijaya Kumar, K. Niwata, T. Hibiya, A. Mizuno, M. Watanabe and Y. Katayama, *Applied Physics Letters* **89** (2006) 241923.